River Flow 2010 - Dittrich, Koll, Aberle & Geisenhainer (eds) - © 2010 Bundesanstalt für Wasserbau ISBN 978-3-939230-00-7

Turbulent Flow over a mildly sloped pool-riffle sequence

T. Stoesser & S. Kara
School of Civil and Environmental Engineering, Georgia Institute of Technology, Atlanta, Georgia, USA

Bruce MacVicar
Department of Civil and Environmental Engineering, University of Waterloo, Waterloo, Canada

James Best
Vent Te Chow Hydrosystems Laboratory, University of Illinois at Urbana-Champaign, USA

ABSTRACT: Large Eddy Simulations (LES) are performed for an open channel flow over a mildly sloped pool-riffle sequence that had been investigated experimentally at the Ven Te Chow hydrosystems laboratory at the University of Illinois at Urbana-Champaign. A train of low-angled (*7.2°*) bedforms were placed in a *60cm* wide rectangular flume at a water-depth-to-bedform-height of *H/k≈1*. The Reynolds number *Re*, based on the bulk velocity *U(bulk)* and the maximum flow depth *H,* is approximately *Re=20,000*. Measured velocities are used to validate the simulations at selected verticals along the centerline of the flume. The code HYDRO3D is used to solve the filtered Navier Stokes equations on a curvilinear non-uniform grid. Overall, good agreement between measured and computed quantities is found. A shear layer forms in the decelerating part of the pool-riffle sequence and alters turbulence intensities considerably. The instantaneous flow field is investigated with emphasis on the occurrence of turbulence structures.

Keywords: *LES, Pool-riffle sequence, Non-uniform flow*

1 INTRODUCTION

Topography of river beds are formed by alternating highs and lows generating the macroscale bedforms such as bars, riffles and pools (Leopold and Wolman, 1957; Montgomery and Buffington, 1997). These bedforms cause changes in the mean velocity, turbulence profiles and in the sediment transport dynamics of the flow (Kironoto and Graf, 1995, Song and Chiew, 2001, MacVicar and Roy, 2007, MacVicar and Rennie, 2008, Yang and Chow, 2008). The turbulence statistics of accelerated or decelerated flow, respectively, differ significantly from uniform flow turbulence statistics due to the non-zero wall-normal velocity component. In the accelerating flow region of the pool, turbulence intensities and shear stresses are enhanced, while in a decelerating flow they are suppressed (Yang and Chow, 2008). These experimental findings imply that the instantaneous flow structures are altered by non-uniformity of the flow.

Ideally, experimental investigations should be complemented with numerical simulations for the further exploration of the mechanisms of the instantaneous flow but also to serve as predictive tools to perform parametric studies. Up to now, only a few numerical simulations of the flow over pool-riffle sequences exist. These are mainly based on the solution of the Reynolds Averaged Navier Stokes (RANS) equations, in which all effects of the turbulent motion must be captured by a turbulence model. One of these studies is the high-resolution 2D simulation performed by Harrison and Keller (2006) on a forced pool-riffle in a boulder-bed stream in southern California. Booker et al. (2001) employed a 3D RANS base CFD model to simulate the hydraulics of a natural pool–riffle sequence. The model calculations were tested against field observations and produced reasonable replications of measured time-averaged velocity directions and magnitudes and in particular velocity profiles. In terms of the instantaneous flow, numerical simulations have so far not significantly advanced the understanding of flows over pool-riffle sequences. However, the success of Large Eddy Simulations (LES) in revealing details of the turbulent flow over smooth walls has recently initiated LES studies of flow over wavy walls (e.g. Calhoun and Street, 2001) or over dunes (Yue et al., 2006; Stoesser et al., 2008). These simulation yielded accurate predictions of the turbulence statistics and revealed the

flow structures over dunes and presented details of the physical mechanisms involved.

In this paper, the flow, second order turbulence statistics as well as longitudinal and near bed turbulence characteristics of a flow over a pool-riffle sequence are examined. Therefore, high-resolution Large-Eddy Simulations are performed and are compared to experimental data obtained in the Ven Te Chow hydrosystems laboratory at the University of Illinois at Urbana-Champaign.

2 NUMERICAL FRAMEWORK

The simulations are performed with the code HYDRO3D-GT. This is a successor of the code HYDRO3D originally developed at Bristol, University (Stoesser, 2002). The code solves the filtered incompressible Navier-Stokes equations on block-structured curvilinear grids using a cell-centered Finite-Volume method with collocated storage of the Cartesian velocity components. Second-order central differences are employed for the convective as well as for the diffusive terms. A fractional-step method is used with a Runge-Kutta predictor and the solution of a pressure-correction equation in the final step as a corrector. The code is parallelized and domain decomposition is used to speed-up the simulation. Message passing between sub-domains is accomplished by MPI.

The dynamic Smagorinsky model first proposed by Germano et al. (1991) is used herein. This model is an extension of the original Smagorinsky model (Smagorinsky, 1963) and makes use of the information available from the smallest resolved scales in the LES.A double filtering procedure leads to a closed expression, commonly referred to as Germano's identity, relating filter stresses at different filter levels to each other. This additional information is then used to determine the model parameter C_s through local averaging.

3 SETUP AND BOUNDARY CONDITIONS

The setup and boundary conditions of the Large Eddy Simulation (LES) were selected in analogy to laboratory experiments that were carried out in the Ven Te Chow hydrosystems lab at the University of Illinois at Urbana-Champaign. In the experiment a train of low-angled (*7.2°*) bedforms, mimicking pool-riffle sequences, were constructed in a *60cm* wide, 30m long rectangular flume (Figure 1). The bedforms were fabricated from Lucite, hence the channel bed can be considered as smooth surface. The water-depth ratio of pool and riffle was approximately H/h=2. The Reynolds number, based on the bulk velocity in the pool, *U(bulk)=0.22m/s*, and the flow depth in the pool, *H=0.115m*, was approximately *Re=20,000*. Primary and secondary flow velocity components were measured over cross sections throughout the flow using vectrino ADVs. Measurements were made at 101 profiles along the channel with 51 points per profile.

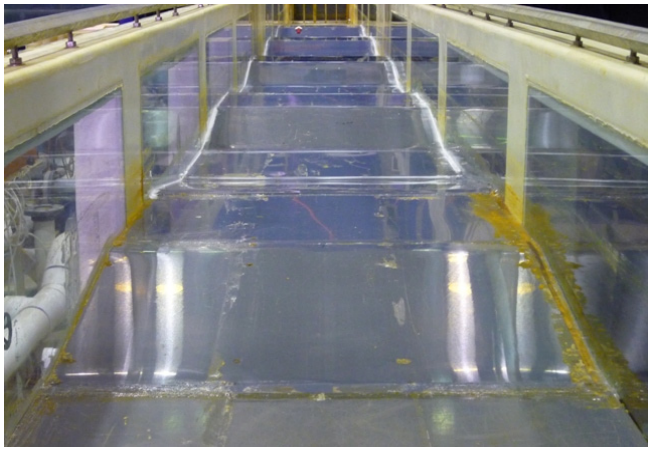

Figure 1. Pool-riffle sequence at the Vent te Chow Hydrosystems Laboratory, University of Illinois at Urbana-Champaign.

The LES domain covered one full pool-riffle sequence in the longitudinal direction and approximately half the width of the flume in the spanwise direction. A geometrically periodic system was created numerically by using cyclic boundary conditions in the flow direction. Cyclic boundary conditions were also applied in the spanwise direction. This treatment was chosen for the sake of reducing the numerical effort of the LES, however it results in neglecting the effects of the sidewalls. For the smooth bed, the no-slip wall boundary condition was employed, with three grid point within the viscous sublayer. The free surface was approximated with a rigid lid at which a slip condition was used. While this treatment does not exactly reproduce the variations of the free surface in the streamwise direction, those are indirectly accounted for by the non-zero dynamic pressure at the rigid lid. A conversion of the distribution of the time- and width-averaged dynamic pressure into a water surface elevation results in a very similar water surface than what was measured (Figure 2).

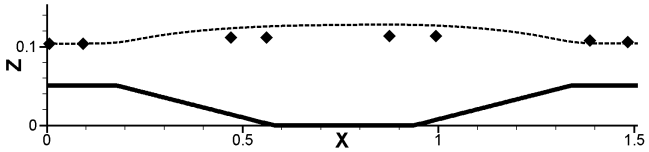

Figure 2. Longitudinal view of the domain with the water surface elevation as measured (dots) and the virtual water surface computed from the dynamic pressure.

The domain was discretized by two different grids in order to examine grid sensitivity. The coarse grid consisted of 321×81×51 (~1.3 million) points whereas the fine grid employed 577×196×101 grid points, which sums to approximately 11.4 million grid points. The grid spacing of the fine grid in terms of wall units is $\Delta x^+ \approx 32$ in the streamwise direction, $\Delta y^+ \approx 18$ in spanwise direction. The spacing near the bed is $\Delta z^+ \approx 1$ and is stretched above the bed towards the free surface. Figure 3 presents a portion of the longitudinal grid, in which only every 5th grid line is plotted.

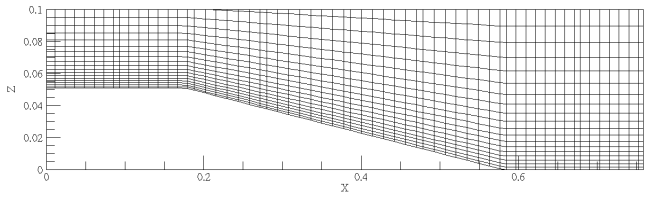

Figure 3. Longitudinal view of the grid of half of the simulation domain (only every fifth grid line is shown)

4 RESULTS AND DISCUSSION

Figure 4 presents streamlines of the time-and spanwise-averaged flow. The mild slope at the upstream side prevents the flow from separating at the crest of the riffle and the velocities decrease gradually along the channel. In the experiment, the flow near the sidewalls exhibit recirculation at the toe of the pool. The presence of sidewalls has a lateral contraction effect on the flow, which will also be shown later (Figures 5 and 6). In the large-eddy simulation sidewalls were not considered, hence the flow exhibits homogeneity in spanwise direction.

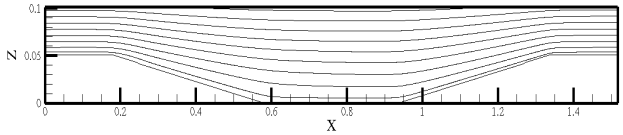

Figure 3. Streamlines of the time-and spanwise-averaged flow

Figure 5 presents time-averaged streamwise velocities of the experiment (upper part) and from the Large-Eddy Simulations (middle) as well as an instantaneous snapshot of the simulated streamwise velocities. The qualitative agreement between measured and simulated velocities is reasonable, especially in the shallow part of the channel. The above mentioned sidewall effect and the associated recirculation at the end of the downslope leads to higher velocities in the pool of the experiment. Hence, an obvious mismatch of velocity magnitude in the LES and the experiment is visible. The instantaneous flow field is characterized by vortical motion, particularly spanwise rollers are detected, and the intermittency of turbulence can be seen. Along the bottom of the pool a low momentum area can be identified. At the riffle crest a shear layer forms, which grows in size above the downward slope. This shear layer clearly exhibits Kelvin-Helmholtz instabilities.

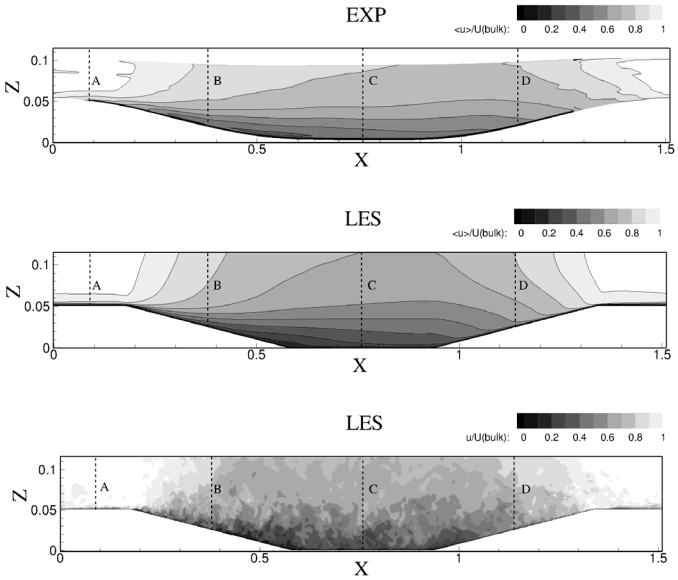

Figure 5. Longitudinal distribution of time-averaged streamwise velocities of the experiment (upper part) and the Large-Eddy simulation (middle) in the center of the flume. Also depicted is a snapshot of the instantaneous streamwise simulation in the same longitudinal plane.

A more quantitative comparison of measured with simulated streamwise velocities is presented in Figure 6. The agreement between measurements (solid dots) and time-averaged LES simulations (solid line represents the fine grid LES, dashed line represents the coarse grid LES) is fairly good especially for Profiles A and D. Underestimation of simulated streamwise velocities in the down-slope and the pool (Profiles B and C) is apparent and is due to aforementioned reasons. Also plotted is the instantaneous velocity profile from the fine grid LES illustrating the prevailing intermittency of the flow. The bulging of the instantaneous profile is a result of near wall streaks (e.g. in Profile B) or sweep and ejection events with locally increased or decreased streamwise velocities, respectively.

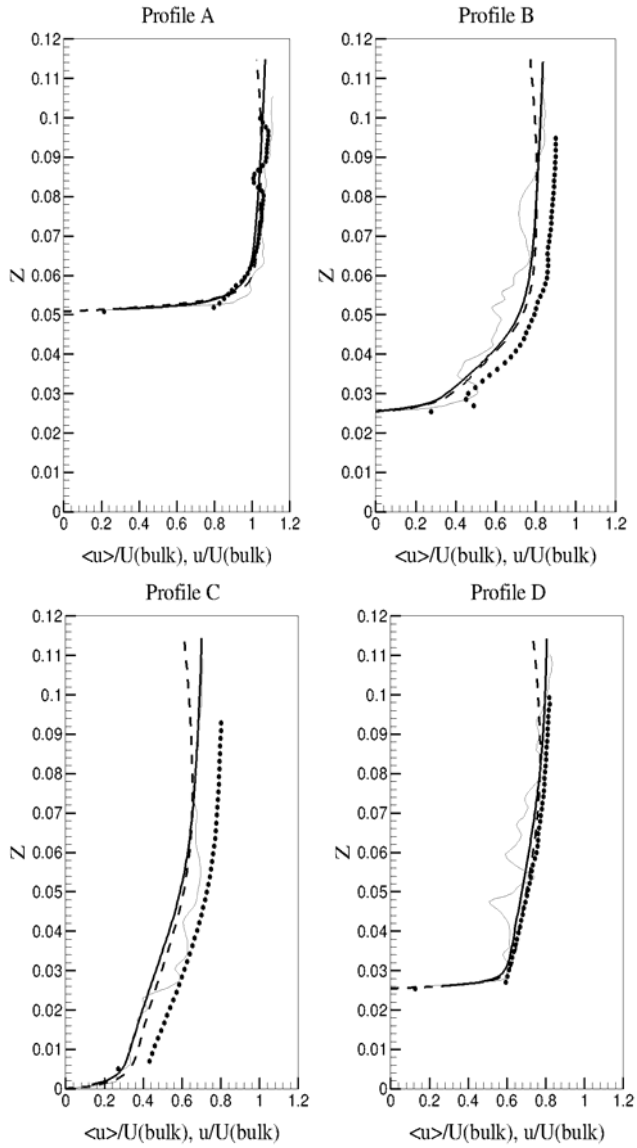

Figure 6. Comparison of simulated time-averaged and instantaneous streamwise velocities with the measured data along four selected profiles. The solid dots represent the measured normalized time-averaged streamwise velocity, while the solid and the dashed black lines represent the results from the fine and coarse grid LES, respectively. Profiles of the instantaneous streamwise velocity of the fine grid LES are plotted as thin gray line.

Figure 7 presents calculated turbulence intensities of all three velocity components. The streamwise turbulence intensity distribution (upper part of Figure 7) underlines the aforementioned increased turbulence in the shear layer on the downslope and in the pool. High values of streamwise turbulence intensity are also found in the boundary layer of the shallow part of the channel. The spanwise and vertical turbulence intensity distribution look very similar. The turbulence intensities attain maximum values along the downslope and in the shear layer and these are considerably higher in the decelerating part of the channel than in the accelerating portion. An area of high spanwise and vertical turbulence is also found near the toe of the slope and near the wall in the pool. Though the pool section of the channel has smaller streamwise velocities than the shallow part of the channel, turbulence levels are enhanced.

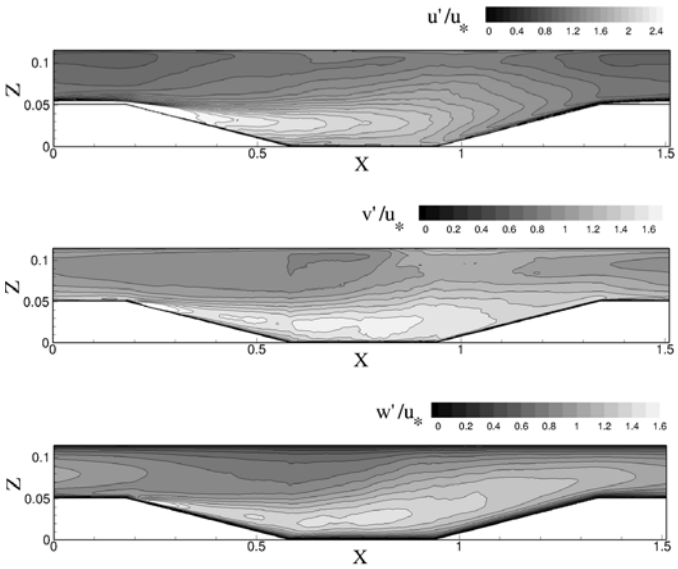

Figure 7. Distribution of streamwise (upper part), spanwise (middle) and wall-normal (lower part) turbulence intensities along the centerline of the channel.

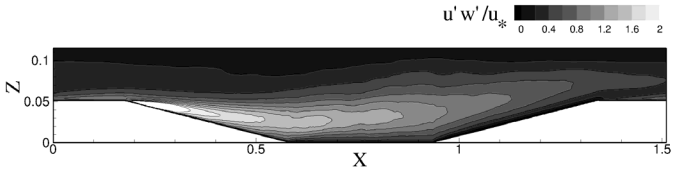

Figure 8. Distribution of the shear stress along the center line of the channel.

Figure 8 shows a longitudinal distribution of the normalized shear stresses along the centerline of the channel. The shear stress is maximum just downstream of the crest, i.e. on the downslope of the channel and exhibits high values almost throughout the pool. These shear stresses are higher than in the boundary layer of the shallow region. The deceleration of the flow along the boundary of the downslope and with higher velocities above creates a shear layer and leads to the formation of turbulence structures in form Kelvin-Helmholtz instabilities.

Figure 9 presents snapshots of the flow visualized with the perturbation velocity vector in a downslope section of the domain (upper part) and in the upslope section of the channel (lower part). The vortical motion, in form of spanwise rollers, is visible and the flow is characterized by sweep and ejection events that are contributing to the shear stress. Though Figure 8 depicts only one instant in time it is obvious that the downslope turbulence is higher than the upslope turbulence, as is shown by the larger perturbation vectors. Similar to the flow in a channel with a uniform depth, vortices are created in the boundary or shear layer, respectively and are transported towards the free surface while weakening.

Figure 10 visualizes above mentioned vortices through contours of the instantaneous spanwise vorticity in a longitudinal plane. The largest values of spanwise vorticity are found in the boundary layer of the shallow part, but also in the shear layer just downstream of the crest. Areas of vortices that are being convected towards the free surface (at an angle of approximately 30 degrees) are apparent in the pool and on the upslope, downstream of the pool. The angle at which these vortices are transported away from the wall is similar to what has been found over smooth and rough walls in channels with a uniform depth.

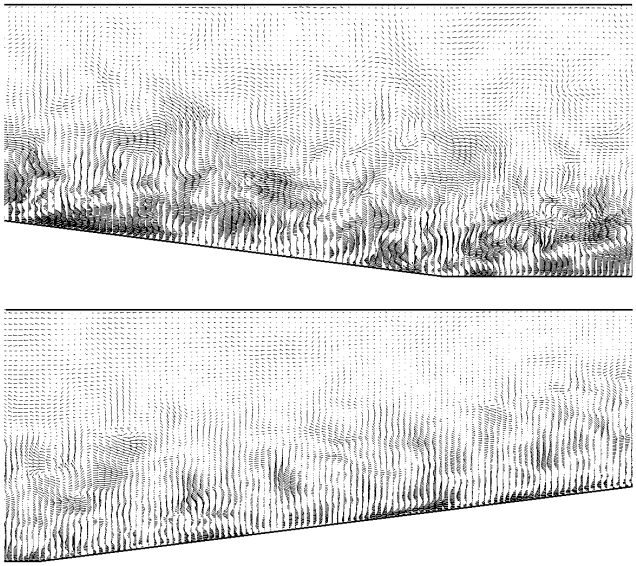

Figure 9. Perturbation vectors at an instant in time for two selected sections of the flow.

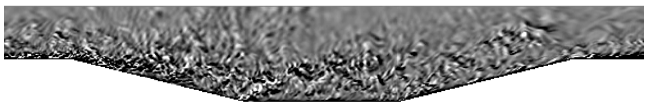

Figure 10. Distribution of the shear stress along the centerline of the channel.

Figure 11 shows a snapshot of near wall streak formation in the pool-riffle sequence as visualized by contours of the instantaneous streamwise velocity perturbation (u'). Streak size and spacing on the upslope and in the shallow part of the channel are very similar, however the near wall flow clearly changes at the crest. Downstream of the crest the near wall seems very unorganized, which is maintained throughout the pool. Once the flow exits the pool nearwall streaks are formed again and are maintained until the next downslope.

Figure 12 shows streaks in the experiment visualized through fine clay particles that are seeded upstream. A good number of particles settle along the edges of the pool-riffle sequence, however the streak formation as shown by the LES matches the particle patterns remarkably well. Coherence of the flow in form of streaks is apparent on the upslope and in the shallow part of the flume, while deposited particles on the downslope and on the bed of the pool due not exhibit any coherence.

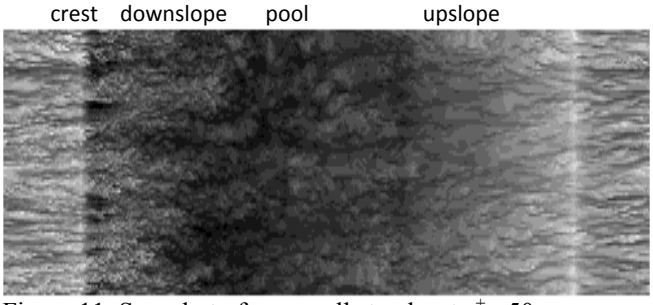

Figure 11. Snapshot of near wall streaks at z^+ =50.

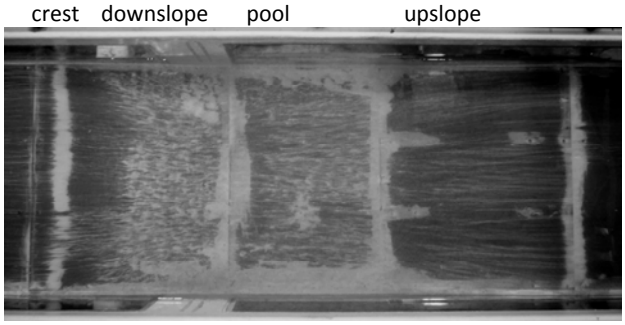

Figure 12. The top view snapshot of pool-riffle sequence from experiment

5 CONCLUSIONS

Large-Eddy Simulations were carried out for the flow in a mildly sloped pool-riffle sequence, which had been investigated experimentally at the Ven Te Chow hydrosystems laboratory at the University of Illinois at Urbana-Champaign. Experimental data were used to validate the LES, though the simulations were performed without sidewalls. Overall, good agreement between measured and computed quantities was found, except in areas where the sidewall considerably affects the flow. A distinct shear layer forms at the crest and grows above the decelerating part of the pool-riffle sequence. This results in turbulence structures in the form of Kelvin-Helmholtz instabilities above the boundary layer on the downslope. Visualized perturbation vectors and contours of instantaneous spanwise vorticity show that increased turbulence is found on the downslope compared with the upslope and the shallow part of the channel. Vortices that are generated in the shear layer are convected towards the free-surface similarly to the flow in channels with a uniform depth. Coherent structures in the form of near wall streaks are present along the upslope and the shallow part of the sequence, flow deceleration and shear layer formation on the downslope seems to lead to a break-up of these streaks, and to incoherence of the flow near the bed in the pool.

The near wall flow is reorganized into streaks along the upslope.

Further analysis is currently underway and more detailed results will be presented at the conference.

REFERENCES

Booker, D. J., Sear, D.A., Payne, A. J. 2001. Modelling three-dimensional flow structures and patterns of boundary shear stress in a natural pool-riffle sequence. Earth Surface Processes and Landforms, 26, 553-576.

Calhoun, R.J., Street, R.L., 2001, Turbulent flow over a wavy surface: Neutral case. Journal of Geophysical Research, Vol. 106(C5), pp. 9277-9294.

Germano, M., Piomelli, U., Moin, P., Cabot, W. 2001. A dynamic subgrid-scale eddy viscosity model. Physics of Fluids, 7(3), 1760-1765.

Harrison, L. R., Keller, E. A. 2006. Modeling forced pool-riffle hydraulics in a boulder-bed stream, southern California. Geomorphology, 83, 232-248.

Kironoto, B. A., Graf, W. H. (1995. Turbulence characteristics in rough non-uniform open-channel flow. Proceedings of the Institution of Civil Engineers-Water Maritime and Energy, 112, 336-348.

Leopold, L. B., Wolman, M. G. 1957. River channel patterns: braided, meandering, and straight. Geological Survey Professional Paper, 282-B, 85 p.

MacVicar, B. J., Roy, A. G. 2007. Hydrodynamics of a forced riffle-pool in a gravelbed river: 1. Mean velocity and turbulence intensity, Water Resources Research, 43, W12401.

MacVicar, B.J., Rennie, C.D. 2009. Lateral distribution of turbulence and secondary currents in non-uniform open channel flow. 33rd IAHR Congress: Water Engineering for a Sustainable Environment, Vancouver, Canada, 1908-1915

Montgomery, D. R., Buffington, J. M. 1997. Channel reach morphology in mountain drainage basins. Geological Society of American Bulletin, 109, 596-611.

Smagorinsky, J. 1963. General circualtion experiments with the primitive equations. Mon. Wea. Rev., 91, 99-164.

Song, T., Chiew, Y. M. 2001. Turbulence measurement in nonuniform open-channel flow using acoustic doppler velocimeter (ADV). Journal of Engineering Mechanics, 127, 219-231.

Stoesser, T. 2002. Development of Validation of a CFD Code for Turbulent Open-Channel Flows. PhD thesis, University of Bristol, UK.

Stoesser, T., Braun, C., Garcia-Villalba, M., Rodi, W., 2008, Turbulence Structures in Flow Over Two Dimensional Dunes, ASCE, Journal Hydr. Engrg. 134(1), pp. 42-55.

Yang, S-Q., Chow, A.T. 2008. Turbulence Structures in non-uniform flows. Advances in Water resources, 31, 1344-1351.

Yue, W., Lin, C.L., Patel, V.C., 2006, Large-Eddy Simulation of Turbulent Flow over a Fixed Two-Dimensional Dune. ASCE, J. Hydr. Engrg., 132(7), pp. 643-651.